

Contents lists available at ScienceDirect

Carbon

journal homepage: www.elsevier.com/locate/carbon



High-power laser-patterning graphene oxide: A new approach to making arbitrarily-shaped self-aligned electrodes



R.D. Rodriguez ^{a, *}, G.V. Murastov ^a, A. Lipovka ^a, M.I. Fatkullin ^a, O. Nozdrina ^a, S.K. Pavlov ^a, P.S. Postnikov ^{a, c}, M.M. Chehimi ^b, Jin-Ju Chen ^d, E. Sheremet ^a

- ^a Tomsk Polytechnic University, Lenina ave. 30, 634034, Tomsk, Russia
- ^b Université Paris Est, UMR 7182 CNRS, UPEC, 94320, Thiais, France
- ^c Department of Solid State Engineering, Institute of Chemical Technology, 16628, Prague, Czech Republic
- ^d School of Materials and Energy, University of Electronic Science and Technology of China, Chengdu, 610054, PR China

ARTICLE INFO

Article history: Received 20 January 2019 Received in revised form 30 April 2019 Accepted 20 May 2019 Available online 22 May 2019

ABSTRACT

We demonstrate the fabrication of self-aligned laser-reduced graphene oxide patterns with a spatial resolution/laser spot size ratio of 1/10, lower than anything reported before using laser-reduction. Laser light modifies graphene oxide (GO) by removing the oxygen-containing groups turning GO into a more graphene-like nanomaterial. Our method is based on high laser power density used for the reduction of GO that results in ablation of the GO film. This enabled us to remove the laser spot illuminated area while inducing the selective graphene oxide reduction at the periphery of the laser spot achieving resistivity of $1.6 \cdot 10^{-5} \,\Omega$ m, as low as values previously reported for other rGO. Therefore, we can exploit laser-induced reduction at high laser power density to pattern GO films with conductive dimensions that are a fraction of the laser spot size. This innovative method is scalable, inexpensive, and straightforward, allowing conductive circuits on arbitrary, flexible, and transparent substrates for applications in lightweight electronics and wearables.

© 2019 Elsevier Ltd. All rights reserved.

1. Introduction

Photonics and light-matter interaction are critical topics for technology nowadays. Thanks to the use of light in telecommunications we have video calls from places located in two opposite sides of the world, doing this at the speed of light. Light has also been playing a fundamental role in driving microelectronics industry development during the last decades. The brains driving our computers and smartphones are made by photolithography, using our ability to focus light on the smallest possible dimensions [1]. This application is a strong technology driver since we always want faster, cheaper, and more robust devices that can work reliably for extended periods. This also implies making devices smaller. However, photolithography as any other optical system is affected by the diffraction limit of light [2]. This limitation is being lately addressed using complex combinations of metamaterials [3] and plasmonic nanostructures [4]. In this work, we demonstrate a new method that allows making

E-mail address: rodriguez@tpu.ru (R.D. Rodriguez).

graphene oxide circuits with light that results in two self-aligned conductive laser-reduced regions that are smaller than the laser spot size. Therefore, this work offers a straightforward and novel way to circumvent the diffraction limit of light in the laser-induced reduction of GO.

Finding a novel way to exploit the properties of reduced graphene oxide is well aligned with the current trends in science and technology that go towards personalized medicine demanding biocompatible, flexible, and "green" electronics [5]. The transition to these technologies requires new materials. In this context, carbon nanomaterials in all their allotropic forms appear to be ideal systems to use in upcoming technological challenges. Graphene oxide (GO) is easily dispersed in water, making it solutionprocessable and compatible with modern fabrication techniques for flexible electronics such as inkjet printing, spraying, spin-, drop-, dip-coating, and so on [6-9]. In contrast to graphene, the presence of oxygen-containing groups (hydroxyl, epoxy, carbonyl, and others) in GO leads to the partial change of hybridization state of carbon from sp² to sp³ [10]. These modifications make GO a scientifically exciting material for a wide range of applications including surface functionalization [11], and what is especially

Corresponding author.

important to the present work, the oxygen groups give GO a dielectric character [12].

The cleavage of oxygen-containing groups drastically changes the electronic and chemical properties of GO and turns it back into a more graphene-like material, the so-called reduced graphene oxide (rGO). In practice, GO reduction could be performed by providing external energy in either a chemical, photochemical, or thermal way [13.14]. The chemical reduction is commonly applied for dispersions of GO and the preparation of large-scale graphene powders. Obviously, since the whole sample gets reduced, this approach cannot be used for the surface patterning of GO and the spatially selective reduction of thin GO films. Moreover, toxic and explosive chemicals such as hydrazine are required in the chemical reaction. Also, the addition of surfactants during GO processing requires the careful purification of the obtained material, which limits the application of rGO in biological systems [10,15,16]. The thermal reduction method requires heating GO to a temperature above 150 °C. At 150–230 °C, the oxygen-containing functional groups transform to volatile compounds (water, CO₂, CO, etc.) and are then partially removed from the surface of graphene followed by the transformation of carbon from sp² to sp³. The annealing temperature to achieve highly conductive rGO films is usually above 1000 °C [13]. The main component is CO₂, other components are CO molecules, H₂O, CH₂O, O₂, and HCOOH in complex with H₂O [17]. For these reasons, thermal annealing is considered a less toxic process than the chemical one. Due to the heat dissipation in GO during the thermal reduction process, this approach, similar to the chemical one, does not enable the creation of patterned GO-rGO microstructures. The resulting rGO also contains the defects that decrease film conductivity [18]. The high defect concentration is because carbon is also partially removed together with the functional groups forming vacancies [17]. The process of GO laser reduction has been intensively studied in several works [13,14,19]. The cleavage of oxygen-containing groups happens due to the combination of a local thermal effect and a photochemical effect, although the influence from each specific mechanism on the overall GO reduction is still a debated issue [20]. Another advantage of the laser-reduction method is the possibility of fine-tuning the reduction degree by changing the laser type and illumination parameters. The most critical factors include laser wavelength, operating mode (pulsed or continuous), pulse duration, power density, and the environment.

Here, using a conventional laser engraving machine, we demonstrate a novel approach to create parallel conductive microstructures with dimensions 1:10 from the laser spot size which is critical to new technological paradigms such as the Internet of Things, wearable, and implantable devices [5,21,22].

2. Experimental

2.1. GO deposition and reduction

A GO dispersion with 4 mg/mL (0.66 vol%) concentration was acquired from Graphenea. The solution was ultrasonicated for 15 min and diluted 2, 4, and 8 times (0.33 vol%, 0.17 vol % and 0.08 vol%, respectively) to obtain four different dispersions. After each dilution process, the GO dispersion was sonicated again for 5 min to prevent the formation of aggregates.

A circuit board with aluminum electrodes for external contacting was used as the substrate for graphene oxide deposition. Before deposition, the board was cleaned using the following procedure: washing with soap, and then in ~5 ml ethanol, 15 min sonicating in ethanol and drying at room conditions following the rinsing with deionized water after each step. The glass substrate was additionally cleaned with acetone. The four GO dispersions (30 μ l volume each) were drop-casted on the circuit board between different Al

electrode pairs as shown in Fig. 3 and dried overnight at room conditions.

Laser patterning was performed using the Minimarker M20 laser engraver with ytterbium pulsed fiber laser ($\lambda=1064~\text{nm}$). For every GO film three groups containing three lines each were engraved, with the power density of $10^6~\text{W/cm}^2$, $5\cdot10^6~\text{W/cm}^2$, and $10^7~\text{W/cm}^2$ respectively. For every group, the lines are 2.7 mm long, and the spacing between them is $150~\mu\text{m}$. All other parameters, including the pulse frequency (90 kHz), scanning speed (500 mm/s), pulse duration (50 ns), and an objective lens with NA = 0.02 were kept constant. The scanning laser engraving system creates a line dot by dot overlapping them with a precision below the laser spot size. Using the mentioned laser engraver parameters, the offset between dots is 5.5 μm , and the laser spot diameter is about 50 μm .

2.2. Atomic force microscopy (AFM) and current sensing AFM (CS-AFM)

For the nanostructures morphology investigation, we used an AFM Integra Prima NT-MDT in semi-contact mode with nonconductive NSG10 tip (NT-MDT). A $100 \times 100~\mu\text{m}^2$ area was measured to obtain the image of two conductive edges, the GO, and the ablated regions in between. The edges conductivity was obtained using CS-AFM in contact mode with a conductive monolithic Au cantilever tip from probes.ters-team.com having curvature radius below 50 nm [23].

We found several issues with the samples obtained on films made using 0.08 and 0.33 vol% concentrations. These problems ranged from bad adhesion and poor electrical contact to the external Al electrodes. The 0.33% vol. sample had the additional issue of a large and rough surface topography which made it impossible to investigate it with our AFM. Therefore, for the precise characterization of rGO microwires, herein we focus on the lines created on 0.17 vol% GO films and irradiated by $10^7 \, \text{W/cm}^2$ power density laser. This concentration resulted in the GO film thickness that made electrically conductive edges and a totally ablated channel between them possible. As an additional benefit, this sample was smooth enough to be investigated locally by atomic force microscopy.

2.3. X-ray photoelectron spectroscopy (XPS) analysis

A Thermo Scientific K Alpha apparatus was employed for XPS analyses. The machine is fitted with a micro-focused monochromatic Al K α X-ray beam (1486.6 eV, 400 μ m spot size) and a flood gun to compensate for the static charge build-up. The samples were clipped on sample holders and outgassed in the fast entry airlock overnight at 2×10^{-7} mbar. The Avantage software, version 5.926, was used for digital acquisition and data processing. The pass energy was set at 50 and 200 eV for the high resolution and the survey spectra, respectively.

The measured sample represents the glass substrate with drop-coated 0.66 vol % GO and laser-reduced area with 3×5 mm size. The XPS study was achieved using both the classical spectral scanning and "snapshot" modes. The latter is a fast mode to acquire spectra during the scanning of the probed surface in horizontal and vertical directions for the evaluation of homogeneity and distribution of surface element concentrations across the reduced area. The horizontal and vertical scanned lines were probed with a 200 μ m spot size, and a distance between spots of 150 μ m for both line scans. The reduction of GO was performed using the same laser system with the following parameters: power density (10^6 W/cm²), pulse frequency (90 kHz), scanning speed (500 mm/s), pulse duration (50 ns), and focusing lens (N.A.: 0.02) were kept constant.

3. Results and discussion

3.1. XPS study

XPS was used to evaluate the chemical composition of rGO and the uniformity of the site-specific reduction process. Due to the spatial resolution limitations of XPS defined by the size of the X-ray spot size, we prepared a dedicated sample for this study with 3×5 mm size on glass. XPS was employed for determining the composition of the central parts of the GO region and the center of the parts that were reduced. By cross-scanning these regions, it was possible to monitor both elemental and chemical changes due to laser-induced reduction. The line scan mode was also very useful in checking patterned surfaces obtained by surface-confined photopolymerization [24] and site-specific photoclick thiolyne reaction [25].

Fig. 1 displays survey (Fig. 1a and b) and high-resolution C1s narrow regions (Fig. 1c and d) from the GO (Fig. 1a and c) and rGO (Fig. 1b and d) parts. The survey region of pristine GO exhibits sharp C1s (285 eV) and O1s (532 eV) peaks; clearly after reduction one can notice a significant decrease in the O1s/C1s relative intensity ratio when going from the oxidized to the reduced region of graphene oxide. The changes in the survey regions also account for specific changes in the fine structure of the high-resolution C1s region. Indeed, the laser-induced reduction does not lead to 100% cleavage of C-O bonds that would result in the total elimination of oxygen atoms, but instead, we still observe the spectral signature from oxidized carbon on the XPS results. Moreover, the freshlyprepared samples were exposed to air which induces reoxidation but at a low extent. The C1s narrow region from GO is fitted with four components (Fig. 1c) centered at 284.6 (sp² carbon), 285.5 (sp³ carbon and C–N bonds), 286.5 (C–O), and 288 eV due to C=0. Interestingly, after reduction, we see a sharp decrease in the relative intensity of the C-O C1s component (Fig. 1d) centered at 286.5 eV. The component centered at 288 eV and assigned to C=0 also undergoes a relative decrease in the relative intensity. The C1s region from reduced GO (Fig. 1d) is actually skewed and exhibits additional peaks assigned to COOR (289 eV) and a π - π * shake up satellite which was screened by the oxidized carbon atoms. The C/O ratio changed from 2.1 to 5.8 going from the pristine to the reduced area of GO. The change in this ratio is due to the reduction of oxidized carbon atoms. The peak-fitted C1s regions (Fig. 1c and d) indicate that the C1s components of the oxidized carbon atoms (C-O at 286.5, C=O at 288 eV and COOR at 289 eV) contribute to 51.2 and 23.1% the total C1s peak areas of pristine and reduced GO, respectively. The distribution analysis of element concentration across the reduced area was carried out using scan mode with 25 points in horizontal and 19 points in the vertical direction as shown in the XPS spectra in Fig. 2a and b. Each XPS spectrum in the line scans was taken at 150 µm steps. The C1s region and C/O ratio across the scan lines are represented in Fig. 2. The spectral analysis demonstrates an excellent reproducibility of the laser-reduction process in different sample regions. The relative standard deviation between C/O ratio did not exceed 2% in the vertical direction and 4% in the horizontal direction. Thus, it can be concluded that the laser-irradiation of GO with the high laser power density here investigated allows achieving the spatially selective formation of

The plot in Fig. 2c shows the horizontal line scan with a change of C/O over a distance of 2500 μm matching the width of the irradiated region. These XPS line scans for vertical and horizontal directions in Fig. 2c further confirm the excellent reproducibility and homogeneity of the laser reduction. Additional spectroscopic characterization by Raman spectroscopy (see Supporting Information) shows the changes that occurred due to the laser-reduction of GO. The Raman spectroscopy results show the D and G spectral region for a sample with the pristine (GO) and the high-power laser irradiated edge (rGO) made with the highest GO concentration of

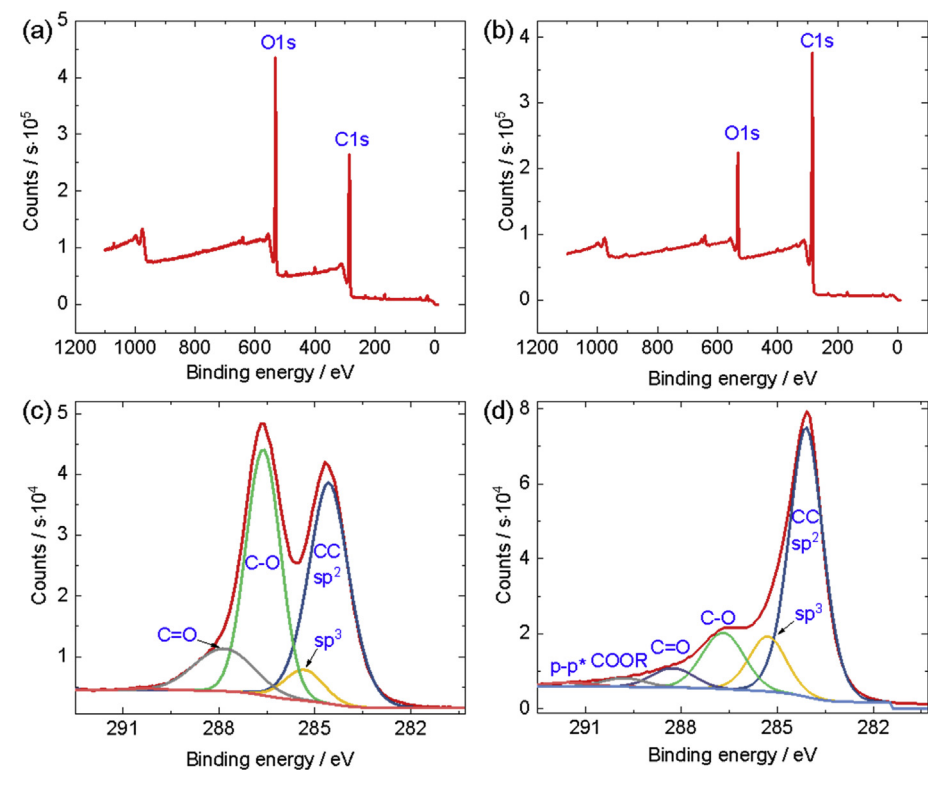
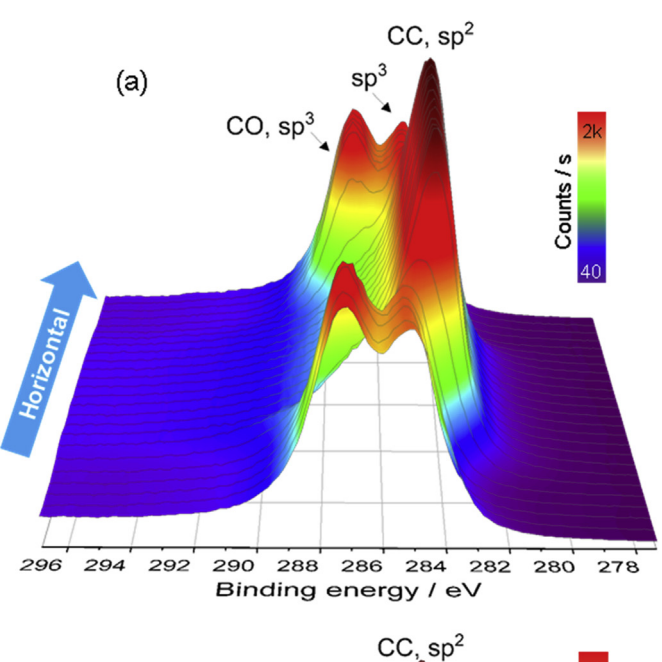
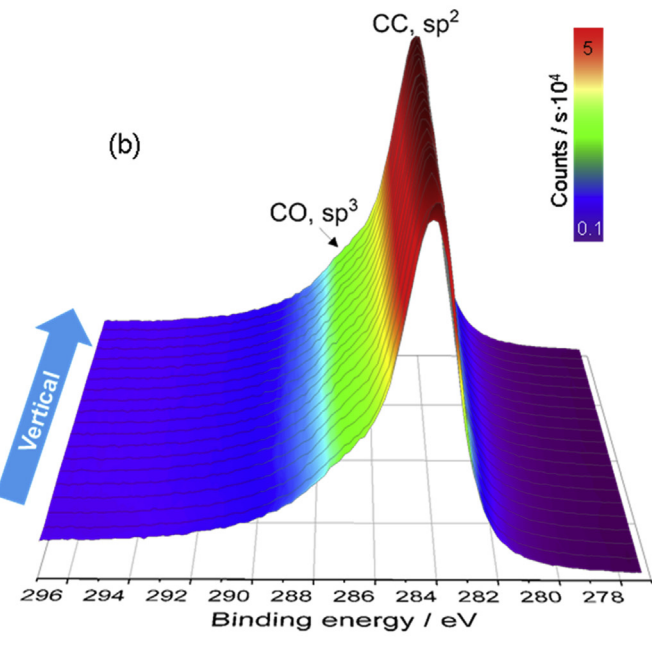


Fig. 1. XPS survey spectra of (a) – pristine GO and (b) – reduced GO; C1s region of (c) – pristine GO and (d) – reduced GO. (A colour version of this figure can be viewed online.)





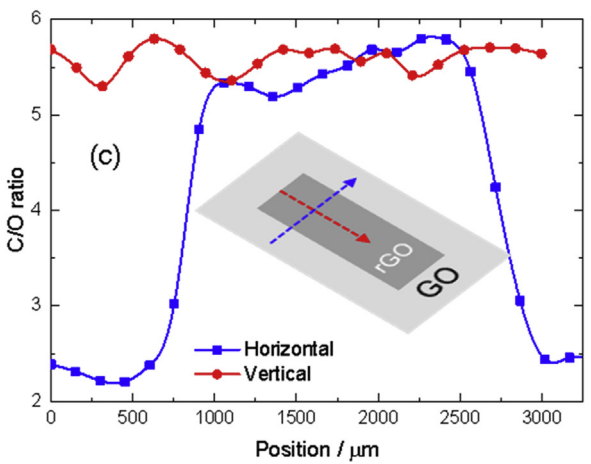


Fig. 2. The XPS data obtained from horizontal (a) and vertical (b) scans of rGO region as indicated in (c). (c) The C/O ratio versus position of moving probe along horizontal and vertical axes of the 3×5 mm rectangle of rGO. The ratio change clearly shows the

0.66 vol %. This concentration was used to minimize the high luminescence signal from the background. Films with lower GO concentration showed a relatively weak Raman signal masked by a strong luminescence from the substrate. Thus, we limited the Raman result to the highest GO concentration that was thick enough to avoid exciting and detecting the background signal. Ma et al. recently showed that the analysis of second-order Raman modes is essential to the investigation of reduction in laserirradiated GO [26]. However, in our case, due to the low intensity of the Raman laser power necessary to minimize the unintentional reduction of GO, the observation of the second-order modes was highly limited. Nevertheless, already the first-order D and G Raman modes provide crucial information about the reduction of GO edges under the high-power laser. The Raman spectra in Fig. S3 show 1) The decrease of D/G intensity ratio by about 20% and 2) the decrease of the D bandwidth by about 55%. These changes for the rGO edge with respect to the pristine film demonstrate the GO reduction under high-power laser irradiation supporting the conclusions from XPS results [14].

3.2. Morphological analysis

After confirming the capability of the laser engraving system to reduce GO films, we performed the GO reduction on the plastic substrate with the highest power density (>10⁶ W/cm²) to deliberately achieve GO ablation. In Fig. 3 the ablation can be clearly seen when applying the $10^7 \,\mathrm{W/cm^2}$ on the 0.17 vol % GO area. This sample was used for the microscale characterization of conductive edges. In the laser engraving system, the laser spot size is about $50 \, \mu m$. We totally ablated a $46.5 \, \mu m$ GO line at the middle of the laser spot where the power density is highest which is understandable considering that the laser beam profile has a Gaussian distribution (Fig. 3b). In Fig. 3b the smooth plastic substrate of about 46.5 µm width can be seen after the GO on top was ablated. The smoothness of the plastic substrate observed by AFM is evidenced in Fig. 3c. This result indicates that there was no substrate modification by the laser that otherwise would be visible as nonuniform crater-like formations due to plastic melting. The GO film thickness was determined by AFM to be up to 300 nm. In a single laser pass, two rGO patterns are formed simultaneously at both sides of the ablated area. The width of these rGO edges is $5-7 \mu m$ that is nearly ten times smaller than the laser spot size. The AFM contrast reaches up to 4.4 µm, with an rGO edge maximum height of 3.5 μ m, and a typical height of 1.33 μ m as shown in Fig. 4d. The thickness increase can be explained by the intense release of gases (mostly CO₂, CO, and water) that leads to the formation of porous structures during the reduction process [17]. This observation is in agreement with previous reports showing that the thickness of rGO films could be 5-20 times larger than the original GO film with a strong dependence on laser power [26–28]. This height increase is also due to a part of rGO material from the ablated region redeposited around the edges. Besides the topographical increase, these edges are also porous which is beneficial for microsupercapacitor applications as shown previously with the laser reduction of hydrated GO films [29].

3.3. rGO conductivity

The resistance evaluated using a conventional multimeter was of 430 kOhm for the 0.17 vol % GO. This sample was also smooth enough to be investigated by CSAFM. On the current map (Fig. 4a

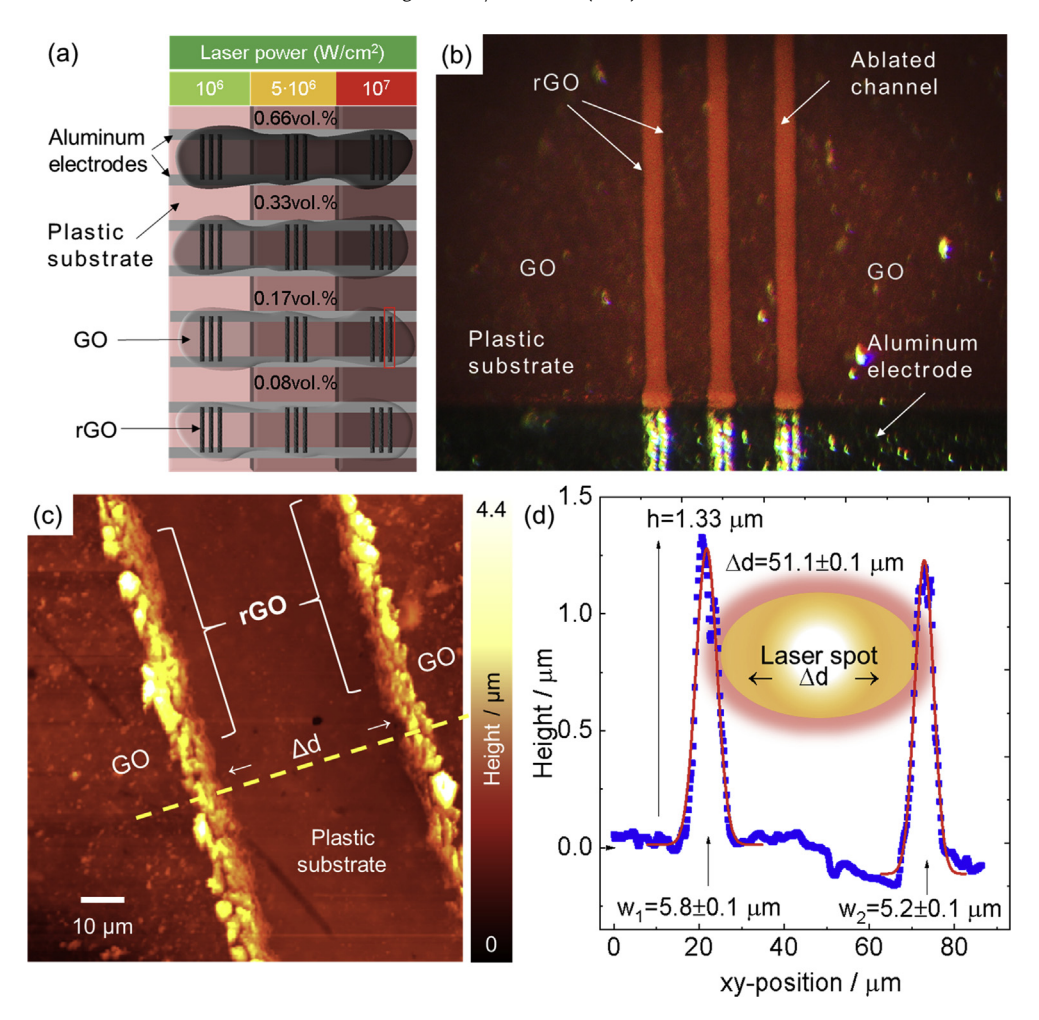


Fig. 3. (a) Sample layout showing the circuit board with Al electrodes for external contact. There are four areas covered with different GO concentrations, and after that, the reduction was performed using three different laser powers as it is shown in the Figure. (b) Optical image of the area where the 0.17 vol% GO concentration was applied and three patterned lines using 10^7 W/cm² power density were created. In the center of each line, we deliberately achieved the GO ablation and only the plastic substrate underneath GO is visible. Due to laser ablation, six rGO wires were formed. The dark red areas at the sides are the plastic substrate covered with GO. The darkest part at the bottom is the aluminum electrode. (c) AFM topography of the engraved line. This multilayer film has a rough surface, unlike the central substrate surface with two protruding rGO lines at the sides. (d) The cross-section of the AFM topography along the dashed line in (d) shows the width of the edges (rGO) and the distance between them. (A colour version of this figure can be viewed online.)

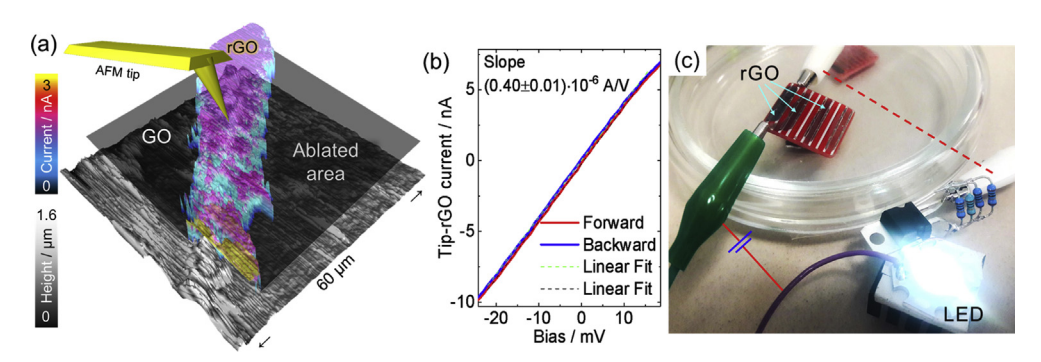


Fig. 4. (a) Current sensing atomic force microscopy results. Topography (grayscale) and conductivity map (color scale) of a single rGO patterned line. (b) IV curves obtained from the rGO line. (c) Photo of the sample; for the practical demonstration of conductivity we used rGO reduced on 0.66% GO area for lighting a LED. (A colour version of this figure can be viewed online.)

and b) we see a single laser-reduced rGO line (obtained at 0.17%, $10^7\,\text{W/cm}^2$) in AFM topography (left) and current map (right). The current map explicitly demonstrates that both GO and ablated areas are not conductive and only the rGO lines are responsible for

the current of up to 3 nA (bias voltage 100 mV). From these results, we see that the width of the conductive line is twice wider than the line observed in the topography image. It is worth noting that this is an apparent width and not the true full-width at half maximum

due to the measurement range limitations of our nano-amperemeter that lead to current saturation. Therefore, the actual width at half maximum of the conductive region is smaller than in Fig. 4a. The heat dissipation beyond the laser spot also contributes to the widening of the conductive part leading to GO reduction beyond the porous edge. Also, the redeposition of ablated material leads to an increase in the conductive area width. Finally, the current distribution is not homogeneous along the line. Moreover, the rough rGO structure is also partly due to the non-uniform GO film thickness obtained by drop-casting. Both these factors affect the electrical conductivity.

The forward and backward I/V sweeps are shown in Fig. 4b. To evaluate the resistivity without being influenced by the contact resistance, the IV characteristics were measured in ten different points along the rGO line (more details are given in the supporting information and Fig. S1). Also, we measured a parallel line at a distance of 50 µm. The IV curves demonstrate ohmic behavior and the resistance decreases as the distance between the two contacts (the tip and the aluminum electrode) is reduced. The two points that have lower resistance occur at 20 µm position where the height of the rGO line is the lowest because of the rough structure. According to our evaluation (see Supporting Information for calculations and Fig. S2) the resistivity value of reduced GO structure is $\rho = 1.6 \cdot 10^{-5} \ \Omega \cdot m$. The sheet resistance for thermally reduced graphene oxide reported in [30] by Wang et al. was recalculated to resistivity given the value $\rho = 1.8 \cdot 10^{-5} \ \Omega \cdot m$. These values are comparable. According to [20] the rGO resistivity is typically in a range from 10^{-2} to $10^{-5} \Omega \cdot m$ meaning that the proposed reduction process offers an rGO material with a competitive rGO conductivity. To further demonstrate the conductivity and stability of the rGO wires, we decided to use them to light a super-bright LED that required a relatively high current density, using the following parameters: $I = 200 \,\mu\text{A}$; $V_{drop} = 2.2 \,\text{V}$; applied voltage 12.5 V (Fig. 4c). We observed the continuous and stable operation of the LED during an extended period using the rGO wires without degradation of the circuit conductivity.

4. Discussion

The XPS results show that the GO films get reduced as evidenced by an increase of the C/O ratio by nearly threefold. The XPS line scans demonstrate the film homogeneity in a large area verifying the scalability of our method. This is not a trivial verification, but it is critical considering that a laser engraver machine is rarely used for the reduction of GO films with such high power densities; one of the few examples was reported recently by Evlashin et al. [31]. The AFM investigation evidenced the ablation of GO in an extension

roughly that of the laser spot size ca. 50 µm. The edges at the laser periphery become reduced instead forming 1D structures with a width nearly 1/10 the laser spot size. This reduction is therefore spatially confined to the outer border of the laser spot. Our conductive CSAFM results in Fig. 4 show the conductive rGO and its spatial confinement to the edges. The anisotropic 1D wires formed along the laser pass are used at the micrometer scale to close a circuit powering a super-bright light emitting diode. The laser spot dimensions determine the feature size in the conventional laser patterning approach of GO, and it mostly does not consider the laser power distribution within the sample's focal plane (see Fig. 5a). In a diffraction-limited system with the numerical aperture of 1, the diffraction limit sets the spatial resolution to approximately half the wavelength. Photolithography is continuously improved by reducing the wavelength towards extreme UV to provide smaller feature sizes required by the microelectronics industry [32]. This has also been pursued by using other irradiation sources such as electrons or X-rays. At the same time, there is a range of imaging methods that enable overcoming this light diffraction limit (e.g. near-field techniques and super-resolution imaging) [33] that do not change the illumination source, but they tend to be more complex and expensive than confocal microscopy. Moreover, those methods to overcome the diffraction limit are definitely non-scalable. Other existing methods for localized rGO patterning use either an atomic force microscopy (AFM) tip [34,35], swift heavy-ion bombardment [36], an electron beam [37], or laser patterning [38]. These methods are effective in achieving GO reduction with a high spatial resolution at the submicrometer level. However, except for the latter, these methods are still costly and not easily scalable. From all of the above, laser irradiation appears to be the most convenient since it is an ecofriendly, precise, easy-to-handle, time-efficient, and inexpensive reduction technology. Until now, the smallest achieved laserreduced GO pattern width (pixel size) is equal to 0.55 μm using a high N.A. objective lens that allowed the authors to create holographic images with a viewing angle of 52° [39]. We anticipate that by using a lens with a high numerical aperture as used in that work, we should be able to beat that record. That is precisely the focus of an ongoing investigation in our group.

We can understand our concept in another way, for example, consider the case of stimulated emission depletion (STED) microscopy as an analogy to the approach we proposed and demonstrated in this work. STED is based on deactivating a part of the fluorophores with a high-power depletion laser leaving only some fluorophores active in a region much smaller than the laser spot size [40]. Similarly, here we exploit the different response of GO on the laser power distribution within a laser spot to inactivate (or

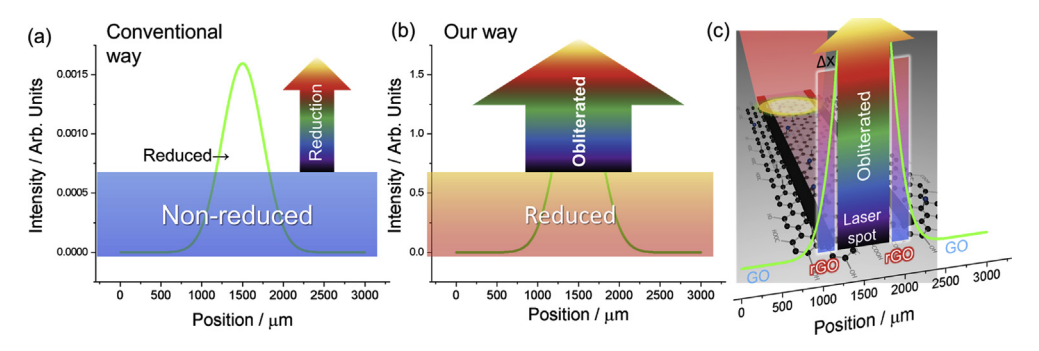


Fig. 5. Illustration of laser reduction approach for GO patterning. The green curve shows the Gaussian profile of a laser beam (intensity in arbitrary units). (a) classical way, only regions at the peak intensity of the Gaussian profile get reduced; (b) Our method, with drastically-higher laser power, ablates the GO at the peak laser beam intensity but leaving the rGO edges around the ablated region. (c) Schematic illustration (non-scaled) summarizing our proposed rGO micropatterning method. (A colour version of this figure can be viewed online.)

rather remove) the GO that otherwise would be reduced resulting in conductive regions with a much larger spatial extension (conventional laser reduction). At the high laser power density used by us, the GO in the middle of the laser spot gets ablated (marked as obliterated in Fig. 5b), this is the analog of the stimulated depletion region in STED. At the borders, around the ablated area, the remaining edges turn into the reduced and electrically conductive rGO material. This is illustrated in the sketch in Fig. 5c where the high power laser passing through the GO film leaves two parallel conductive lines of rGO. It is worth noticing that in this work, we optimized the irradiation parameters and GO concentration to obtain isolated rGO nanowires (with total ablation of GO beneath the laser spot) that were smooth enough to be investigated by AFM. The interdependence of the final sample characteristics (rGO uniformity and smoothness, GO ablation, and rGO conductivity) is an important but complex problem that requires a dedicated investigation of its own in follow up works.

The creation of an ablated region in between is technologically interesting since it provides a reliable way to electrically separate the two conductive edges obtained by laser processing in a single step.

5. Conclusion

We demonstrated a new promising approach to the formation of highly conductive rGO patterns using a scalable and straightforward method with high-power laser irradiation in ambient conditions. The primary use of the laser tool device (laser cutting) was diverted to a different application with impact in future nanotechnologies. The rGO-microwires obtained with our method are much smaller than the laser spot size and represent two parallel self-aligned conductors with a constant separation distance given by the laser spot size. The formation of parallel conductive electrodes could be beneficial for some applications like as interdigitated electrodes and as electrodes separated by a constant channel for field-effect transistor applications. This separation distance and the width of the rGO wire could be controlled by the laser spot size which depends on the optics used, focusing conditions, and power. The role of these parameters could be investigated in future works, that also take into account the role of laser wavelength. This method could be useful in terms of precise electrical circuits development in microelectronics. By minimizing the laser spot size, it may be possible to achieve rGO patterns of nanometer size which is now an ongoing investigation to obtain record-sized rGO circuits by laser irradiation on flexible substrates.

Acknowledgments

We are very grateful to Alexey Yakovlev, Elena Polysadova, and Mekhman Yusubov for their essential support that made this research possible. We are thankful to Ammar Al-Hamry, Varnika Prakash, and Olfa Kanoun for providing the GO material and for fruitful discussions. We also thank Vladimir Sypchenko for assistance with the Raman spectrometer. This research was funded by the Tomsk Polytechnic University Competitiveness Enhancement Program 5–100.

Appendix A. Supplementary data

Supplementary data to this article can be found online at https://doi.org/10.1016/j.carbon.2019.05.049.

References

[1] S. Jesse, A.Y. Borisevich, J.D. Fowlkes, A.R. Lupini, P.D. Rack, R.R. Unocic,

- B.G. Sumpter, S.V. Kalinin, A. Belianinov, O.S. Ovchinnikova, Directing matter: toward atomic-scale 3D nanofabrication, ACS Nano 10 (2016) 5600—5618.
- [2] T. Ito, S. Okazaki, Pushing the limits of lithography, Nature 406 (2000) 1027–1031.
- [3] J. Sun, N.M. Litchinitser, Toward practical, subwavelength, visible-light photolithography with hyperlens, ACS Nano 12 (2018) 542–548.
- [4] W. Kong, Y. Luo, C. Zhao, L. Liu, P. Gao, M. Pu, C. Wang, X. Luo, Plasmonic interference lithography for low-cost fabrication of dense lines with sub-50 nm half-pitch, ACS Appl. Nano Mater. (2019), https://doi.org/10.1021/ acsanm.8b02047.
- [5] E. Singh, M. Meyyappan, H.S. Nalwa, Flexible graphene-based wearable gas and chemical sensors, ACS Appl. Mater. Interfaces 9 (2017) 34544–34586.
- [6] Y. Su, V.G. Kravets, S.L. Wong, J. Waters, A.K. Geim, R.R. Nair, Impermeable barrier films and protective coatings based on reduced graphene oxide, Nat. Commun. 5 (2014) 4843.
- [7] L.T. Le, M.H. Ervin, H. Qiu, B.E. Fuchs, W.Y. Lee, Graphene supercapacitor electrodes fabricated by inkjet printing and thermal reduction of graphene oxide, Electrochem. Commun. 13 (2011) 355–358.
- [8] R.R. Nair, H.A. Wu, P.N. Jayaram, I.V. Grigorieva, A.K. Geim, Unimpeded permeation of water through helium-leak-tight graphene-based membranes, Science 335 (2012) 442–444.
- [9] H.W. Kim, H.W. Yoon, S.-M. Yoon, B.M. Yoo, B.K. Ahn, Y.H. Cho, H.J. Shin, H. Yang, U. Paik, S. Kwon, J.-Y. Choi, H.B. Park, Selective gas transport through few-layered graphene and graphene oxide membranes, Science 342 (2013) 91–95
- [10] H.C. Schniepp, J.-L. Li, M.J. McAllister, H. Sai, M. Herrera-Alonso, D.H. Adamson, R.K. Prud'homme, R. Car, D.A. Saville, I.A. Aksay, Functionalized single graphene sheets derived from splitting graphite oxide, J. Phys. Chem. B 110 (2006) 8535–8539.
- [11] L. Dedelaite, R.D. Rodriguez, E. Andriukonis, M. Hietschold, D.R.T. Zahn, A. Ramanavicius, Surfaces functionalized by graphene oxide nanosheets for single cell investigations, Sensor. Actuator. B Chem. 255 (2018) 1735–1743.
- [12] Y. Zhu, S. Murali, W. Cai, X. Li, J.W. Suk, J.R. Potts, R.S. Ruoff, Correction: graphene and graphene oxide: synthesis, properties, and applications, Adv. Mater. 22 (2010) 3906–3994.
- [13] S. Pei, H.-M. Cheng, The reduction of graphene oxide, Carbon N. Y. 50 (2012) 3210–3228.
- [14] A. Al-Hamry, H. Kang, E. Sowade, V. Dzhagan, R.D. Rodriguez, C. Müller, D.R.T. Zahn, R.R. Baumann, O. Kanoun, Tuning the reduction and conductivity of solution-processed graphene oxide by intense pulsed light, Carbon N. Y. 102 (2016) 236–244.
- [15] S. Park, J. An, J.R. Potts, A. Velamakanni, S. Murali, R.S. Ruoff, Hydrazine-reduction of graphite- and graphene oxide, Carbon N. Y. 49 (2011) 3019–3023
- [16] S. Stankovich, D.A. Dikin, R.D. Piner, K.A. Kohlhaas, A. Kleinhammes, Y. Jia, Y. Wu, S.T. Nguyen, R.S. Ruoff, Synthesis of graphene-based nanosheets via chemical reduction of exfoliated graphite oxide, Carbon N. Y. 45 (2007) 1558—1565.
- [17] Y.M. Shulga, N. Yu Shulga, Y.N. Parkhomenko, Carbon nanostructures reduced from graphite oxide as electrode materials for supercapacitors, izvestiya vysshikh uchebnykh zavedenii, in: Materialy Elektronnoi Tekhniki = Materials of Electronics Engineering, 2015, p. 157.
- [18] A. Pulido, P. Concepción, M. Boronat, C. Botas, P. Alvarez, R. Menendez, A. Corma, Reconstruction of the carbon sp2 network in graphene oxide by low-temperature reaction with CO, J. Mater. Chem. 22 (2012) 51–56.
- [19] R. Trusovas, G. Račiukaitis, G. Niaura, J. Barkauskas, G. Valušis, R. Pauliukaite, Recent advances in laser utilization in the chemical modification of graphene oxide and its applications, Advanced Optical Materials 4 (2015) 37–65.
- [20] Z. Wan, E.W. Streed, M. Lobino, S. Wang, R.T. Sang, I.S. Cole, D.V. Thiel, Q. Li, Laser-reduced graphene: synthesis, properties, and applications, Adv. Mater. Technol. (2018), https://doi.org/10.1002/admt.201700315.
- [21] H.J. Park, W.-J. Kim, H.-K. Lee, D.-S. Lee, J.-H. Shin, Y. Jun, Y.J. Yun, Highly flexible, mechanically stable, and sensitive NO2 gas sensors based on reduced graphene oxide nanofibrous mesh fabric for flexible electronics, Sensor. Actuator. B Chem. 257 (2018) 846–852.
- [22] G. Rajitha, R.K. Dash, Optically transparent and high dielectric constant reduced graphene oxide (RGO)-PDMS based flexible composite for wearable and flexible sensors, Sens. Actuators A Phys. 277 (2018) 26–34.
- [23] R.D. Rodriguez, E. Sheremet, S. Müller, O.D. Gordan, A. Villabona, S. Schulze, M. Hietschold, D.R.T. Zahn, Compact metal probes: a solution for atomic force microscopy based tip-enhanced Raman spectroscopy, Rev. Sci. Instrum. 83 (2012) 123708.
- [24] I. Bakas, G. Yilmaz, Z. Ait-Touchente, A. Lamouri, P. Lang, N. Battaglini, B. Carbonnier, M.M. Chehimi, Y. Yagci, Diazonium salts for surface-confined visible light radical photopolymerization, J. Polym. Sci. A Polym. Chem. 54 (2016) 3506–3515.
- [25] M. Bengamra, A. Khlifi, N. Ktari, S. Mahouche-Chergui, B. Carbonnier, N. Fourati, R. Kalfat, M.M. Chehimi, Silanized aryl layers through thiol-yne photo-click reaction, Langmuir 31 (2015) 10717—10724.
- [26] B. Ma, R.D. Rodriguez, A. Ruban, S. Pavlov, E. Sheremet, The correlation between electrical conductivity and second-order Raman modes of laser-reduced graphene oxide, Phys. Chem. Chem. Phys. (2019), https://doi.org/10.1039/c9cp00093c.
- [27] L.V. Thekkekara, B. Jia, Y. Zhang, L. Qiu, D. Li, M. Gu, On-chip energy storage integrated with solar cells using a laser scribed graphene oxide film, Appl.

- Phys. Lett. 107 (2015), 031105, https://doi.org/10.1063/1.4927145.
- [28] T.X. Tran, H. Choi, C.H. Che, J.H. Sul, I.G. Kim, S.M. Lee, J.H. Kim, J.B., In, laserinduced reduction of graphene oxide by intensity-modulated line beam for supercapacitor applications, ACS Appl. Mater. Interfaces 10 (2018) 39777-39784.
- [29] W. Gao, N. Singh, L. Song, Z. Liu, A.L.M. Reddy, L. Ci, R. Vajtai, Q. Zhang, B. Wei, P.M. Ajayan, Direct laser writing of micro-supercapacitors on hydrated graphite oxide films, Nat. Nanotechnol. 6 (2011) 496–500.
- [30] X. Wang, L. Zhi, K. Müllen, Transparent, conductive graphene electrodes for dye-sensitized solar cells, Nano Lett. 8 (2008) 323–327.
- [31] S. Evlashin, P. Dyakonov, R. Khmelnitsky, S. Dagesyan, A. Klokov, A. Sharkov, P. Timashev, S. Minaeva, K. Maslakov, S. Svyakhovskiy, N. Suetin, Controllable laser reduction of graphene oxide films for photoelectronic applications, ACS Appl. Mater. Interfaces 8 (2016) 28880–28887.
- [32] Rodolfo Cruz-Silva, Jiaxing Huang, Laura J. Cote, Flash reduction and patterning of graphite oxide and its polymer composite, J. Am. Chem. Soc. 131 2009) 11027–11032.
- [33] Principles of Nano-Optics, Nano Today 1 (2006) 41.
 [34] J.M. Mativetsky, E. Treossi, E. Orgiu, M. Melucci, G.P. Veronese, P. Samorì, V. Palermo, Local current mapping and patterning of reduced graphene oxide, J. Am. Chem. Soc. 132 (2010) 14130—14136. [35] Z. Wei, D. Wang, S. Kim, S.-Y. Kim, Y. Hu, M.K. Yakes, A.R. Laracuente, Z. Dai,

- S.R. Marder, C. Berger, W.P. King, W.A. de Heer, P.E. Sheehan, E. Riedo, Nanoscale tunable reduction of graphene oxide for graphene electronics, Science 328 (2010) 1373-1376.
- [36] A. Olejniczak, N.A. Nebogatikova, A.V. Frolov, M. Kulik, I.V. Antonova, V.A. Skuratov, Swift heavy-ion irradiation of graphene oxide: localized reduction and formation of sp-hybridized carbon chains, Carbon N. Y. 141 (2019) 390-399.
- [37] G. Gonçalves, J. Borme, I. Bdkin, A. González-Mayorga, G. Irurueta, H.I.S. Nogueira, M.C. Serrano, P. Alpuim, A.A. Paula, Reductive nanometric patterning of graphene oxide paper using electron beam lithography, Carbon N. Y. 129 (2018) 63–75.
- [38] Yonglai Zhang, Li Guo, Wei Shu, Yinyan Hec, Hong Xia, Qidai Chenb, Hong-Bo Sunb, Feng-Shou Xiao, Direct imprinting of microcircuits on graphene oxides film by femtosecond laser reduction, Nano Today 5 (2010), https:// doi.org/10.1016/j.nantod.2009.12.009 online 19 January.
- [39] X. Li, H. Ren, X. Chen, J. Liu, Q. Li, C. Li, G. Xue, J. Jia, L. Cao, A. Sahu, B. Hu, Y. Wang, G. Jin, M. Gu, Athermally photoreduced graphene oxides for three-dimensional holographic images, Nat. Commun. 6 (2015) 6984.
- [40] S. Hell (Ed.), Optics Far beyond the Diffraction Limit: Stimulated Emission Depletion Microscopy, Springer Handbook of Lasers and Optics, 2007, pp. 1091-1098.